The Current Understanding of the Trap Generation Mechanisms that Lead to the Power Law Model for Gate Dielectric Breakdown

Paul E. Nicollian, Anand T. Krishnan, Cathy A. Chancellor, Rajesh B. Khamankar, Srinivasan Chakravarthi, Chris Bowen, and Vijay K. Reddy

Texas Instruments Incorporated
Silicon Technology Development
MS 366, 13121 TI Boulevard; Dallas, Texas 75243
Tel: (972)-995-2820; fax: (972)-995-1724; email: nicollian@ti.com

ABSTRACT

This paper reviews recent experiments that have shown that the probable mechanism for low voltage trap generation and dielectric breakdown is anode hydrogen release. Vibrational excitation of silicon-hydrogen bonds is the process that provides the most plausible explanation for the existence of a power law model for TDDB.

INTRODUCTION

Gate dielectrics continue to be aggressively scaled to meet high performance requirements. In recent years, the reduction in operating voltage with time has slowed significantly to push performance to even higher levels. Figure 1 compares the 2001 and 2004 ITRS roadmaps for V_{CC} scaling [1]. For a fixed EOT, the slowing of V_{CC} scaling shown in Figure 1 will erode t_{BD} by ~ 10 to 13 orders of magnitude by the year 2013, with possibly more degradation for high performance devices. Since TDDB is a strongly voltage driven phenomenon [2], the slowing of voltage scaling has become a significant new challenge for meeting gate dielectric reliability requirements.

To address this problem, a power law model for t_{BD} vs. gate voltage has been proposed [2]. This model has a power law exponent greater than 40, which was inexplicably large when it was first introduced. Due to the need to implement this model to meet state of the art reliability requirements, there has been significant interest in deriving an explanation for the existence of a TDDB power law. The primary mechanisms that are thought to be responsible for breakdown are anode hydrogen release (AHR) [3] and anode hole injection (AHI) [4,5]. Accordingly, these processes have been extensively studied.

In this work, we will review recent progress in understanding the physical mechanisms that result in a power law dependence of the time to breakdown on gate voltage. We will show that while holes remain involved in the processes that lead to trap generation, anode hole injection is not the cause for breakdown at low voltages. We will present experimental evidence that points to anode hydrogen release as the process that triggers trap generation and breakdown. Two hydrogen species (H^+ and H^0) are involved. After comparing results from scanning tunneling microscopy experiments (STM) with data from breakdown studies, we will show that the TDDB power law model arises from vibrational excitation of silicon hydrogen bonds. We will discuss the impact of vibrational excitation on the trap configurations that cause breakdown.

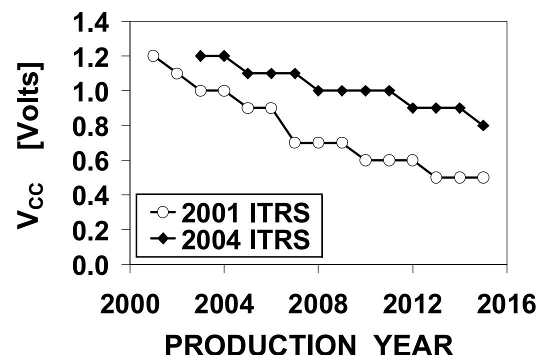

Figure 1. Comparison of 2001 and 2004 ITRS roadmaps for operating voltage. After ITRS roadmaps, Ref. [1].

RESULTS

Characteristics of the TDDB power law model

The breakdown of ultra thin dielectrics has been shown to be gate voltage (energy) driven at low voltages [6-8]. There are two formulations for gate voltage driven breakdown: The exponential law and power law. They are defined respectively in equations (1) and (2).

$$t_{BD} = t_0 e^{-\gamma V_g} \quad (1)$$

$$t_{BD} = a V_G^{-N} \quad (2)$$

γ is the voltage acceleration factor. Similar relationships can be written for Q_{BD}. From (1) and (2), data following the exponential model will result a straight line on a semi-log plot of t_{BD} vs. V_G, whereas the power law model yields a straight line in a log-log graph of t_{BD} vs. V_G. Data are plotted using exponential and power law scaling in Figures 2 and 3 respectively [2]. In Figure 2, it can be seen that the lines corresponding to the least squares fits (LSF) of the data are not parallel for different areas. Extrapolations to low voltages yield the unrealistic result that devices with large areas can

1-4244-0919-5/07/$25.00 ©2007 IEEE

IEEE 07CH37867 45th Annual International Reliability Physics Symposium, Phoenix, 2007

Authorized licensed use limited to: PORTLAND STATE UNIVERSITY. Downloaded on May 22, 2009 at 00:57 from IEEE Xplore. Restrictions apply.

have longer lifetimes than smaller areas. This violates Weibull scaling of the time to breakdown with gate area, where [9]

$$t_{BD}(2)/t_{BD}(1) = (A_1/A_2)^{1/\beta} \quad (3)$$

β is the Weibull slope, or shape parameter. In contrast, using the same data as in Figure 2, devices with different areas form parallel lines in the log-log scale in Figure 3. Accordingly, the power law model is consistent with Weibull scaling. The voltage acceleration factor is defined as

$$AF = -\partial \ln(t_{BD})/\partial V_G \quad (4)$$

The exponential law voltage acceleration factor γ is independent of voltage, while the power law voltage acceleration factor is N/V_G and increases with decreasing voltage. In Figure 4, the acceleration factors for SiON films ranging in thickness from 10Å to 32Å show the V_G^{-1} dependence expected for a power law model. Accordingly, from Figures 2-4, the power law appears to be the more plausible model. However, the power law exponent "N" is inexplicably high; approximately 48 as shown in Figure 4. We will analyze this puzzling behavior in this paper.

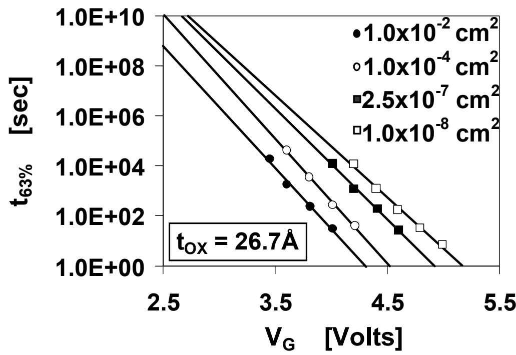

Figure 2. Semi-log plot of time to breakdown vs. gate voltage. After Wu, Ref. [2].

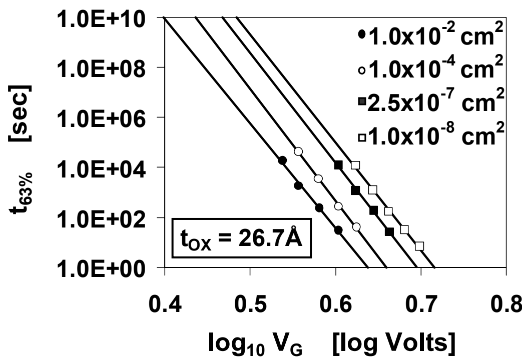

Figure 3. Log-log plot of time to breakdown vs. gate voltage for the same data used in Figure 2. After Wu, Ref. [2].

Features of anode hole injection

Anode hole injection occurs when electrons arriving at the anode dissipate their energy via impact ionization and impart sufficient energy to holes so that they are injected into the oxide valence band [4,5]. This process is shown for an inverted NMOS device in Figure 5. The injected holes can subsequently generate electrons traps, hole traps, and interface traps, or be captured by as-grown centers [10-12]. AHI has an energy threshold E_{TH} of about 6eV. This includes the ~ 1.1eV energy required to generate an electron hole pair plus the valence band offset between silicon and oxide.

$$E_{TH} \approx \varphi_H + E_G(Si) \approx 4.8eV + 1.1eV \approx 6eV \quad (5)$$

The average and maximum kinetic energy of holes in the anode created through impact ionization are respectively

$$E(h_1)_{AVG} \approx qV_{OX} - 1.1eV \quad (6)$$

$$E(h_1)_{MAX} \approx qV_G - 1.1eV \quad (7)$$

Either $E(h_1)_{AVG}$ or $E(h_1)_{MAX}$ must be greater than ~ 5 eV (the hole barrier height) for anode hole injection to occur.

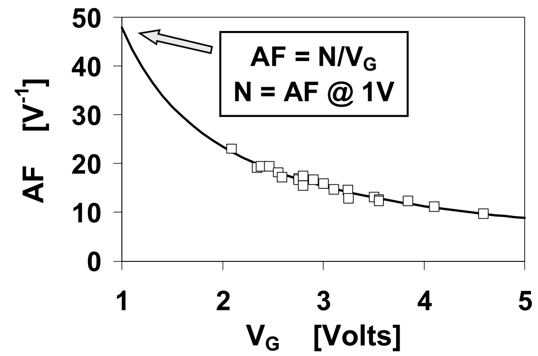

Figure 4. Voltage acceleration factors for SiON films ranging from 10Å to 32Å EOT. The power law exponent "N" is approximately 48 for this dataset.

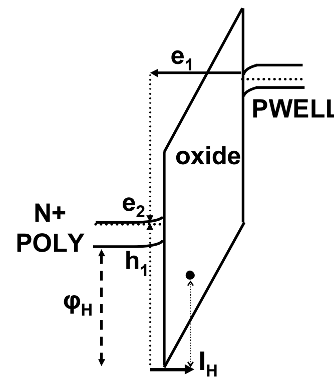

Figure 5. Band diagram for anode hole injection in an inverted NMOS device. Electron e_1 tunnels into the anode and impact ionizes to produce e_2 and h_1. If h_1 acquires > 5eV kinetic energy in the anode, it will be injected into the oxide.

The process shown in Figure 5 is known as majority ionization [13]. The final states of both e_1 and e_2 lie in the poly conduction band. Majority ionization still occurs for

Authorized licensed use limited to: PORTLAND STATE UNIVERSITY. Downloaded on May 22, 2009 at 00:57 from IEEE Xplore. Restrictions apply.

V_{OX} < 6V, but at a lower rate. Since the maximum energy of electrons in the anode is qV_G [6], majority ionization remains an operative process down to a gate voltage of about 6V.

If holes are present in the anode electrode, i.e. $V_G < 0$, then a process called minority ionization can result in anode hole injection, where electrons entering the anode transfer their kinetic energy to free holes [13]. While this effect occurs at a lower rate than majority ionization, it enables hole injection at lower voltages because tunneling electrons do not have to lose 1.1eV to generate electron-hole pairs when free holes are already present. There are two types of minority ionization: (a) One electron final state in the anode valence band; (b) Two electron final states in the anode valence band. The maximum hole kinetic energies for (a) and (b) are respectively [13]

$$E(h_1)_{MAX} = qV_G + |E_F - E_V| \quad (8)$$

$$E(h_1)_{MAX} = qV_G + 2|E_F - E_V| + 1.1eV \quad (9)$$

Equation (9) predicts that it is still possible to get AHI at V_G ~ 3.5V. Experiments have confirmed that this is a plausible theory [7]. However, explaining breakdown as due to anode hole injection at lower voltages in inverted NMOS is problematic. Accordingly, anode hydrogen release is expected to play a central role in breakdown at low voltages. We will re-visit anode hole injection at low voltages later in this work.

Features of anode hydrogen release

Anode hydrogen release occurs when the dissipation of the energy of electrons arriving at the anode results in the desorption of hydrogen [3]. This process results in the creation of bulk electron traps as well as interface states at both interfaces [3], as shown in Figure 6.

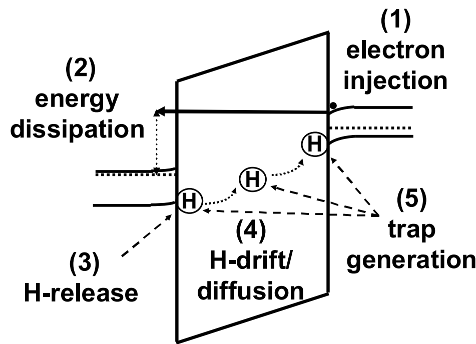

Figure 6. Band diagram for AHR. A hydrogen species is released in the processes that dissipate the energy of tunneling electrons that have entered the anode. The desorption of hydrogen results in bulk and interface trap generation.

AHR is strongly dependent on temperature and weakly dependent on thickness [3]. Similar to AHI, the threshold energy for AHR is thought to be 6eV. However, STM experiments have shown that the threshold energy for hydrogen release ranges from 2.5eV to 7eV [14]; depending on the desorption mechanism. Another gap in the understanding of anode hydrogen release is that until recently, neither the reaction leading to AHR nor the hydrogen species desorbed from the anode were elucidated. We will review these experiments in a later section.

Reaction-diffusion theory

Trap creation is the product of an electrochemical reaction. Accordingly, reaction-diffusion theory [15] is a useful tool in analyzing defect generation in the Si-SiO_2 and Si-SiON systems. Trap generation follows a power law in fluence:

$$N(Q) = bQ^m \quad (10)$$

Reaction-diffusion theory can be used to determine the hydrogen species released from the trap generation power law "m" in equation (10) when the system is in quasi-equilibrium [15]. The characteristics of quasi-equilibrium is a system where dN/dQ (or dN/dt) is small because both forward reaction (trap generation) and reverse reaction (recovery) are operative and are similar in magnitude. The test for quasi-equilibrium is that if measurable recovery effects are present, a delay time between stress and sense will result in a larger trap generation power law "m" [16]. This cannot be explained by hole de-trapping, as this effect would be reduced at the lower field resulting from interrupting the stress. The trap generation power law exponent "m" resultant from the hydrogen species released is shown in Figure 7. Note that only charged species result in m > 1/4. In the following section, we will show that reaction diffusion theory applies to NMOS TDDB and elucidate the reactions leading to trap generation.

reaction product	m	reference
H_2	1/6	[17]
H^0	1/4	[15]
H_2^+	1/3	[18]
H_2^-	1/3	[18]
H^+	1/2	[19]
H^-	1/2	[19]

Figure 7. Trap generation power law exponents calculated with reaction-diffusion theory. In addition to the above references, elegant derivations are given in Alam, Ref. [18].

Identification of the hydrogen species that cause trap generation in ultra thin SiON dielectrics

Reliability models for the NMOS on-state are of particular importance because in an inverter, the entire gate oxide area is stressed. A problem with the analysis of degradation mechanisms for this mode is that the anode, where the reactions initiate, is the poly-SiON interface, which is difficult to characterize directly. To circumvent this problem, a known reaction is initiated at the readily characterized Si-SiON interface and used as a probe of the anode reactions [20]. This is accomplished by applying a back-bias to the pwell to induce the desorption of cathode hydrogen by substrate hot electrons as shown in Figure 8. No n+ injector is used to avoid both uncontrolled flooding of the dielectric with the cathode

Authorized licensed use limited to: PORTLAND STATE UNIVERSITY. Downloaded on May 22, 2009 at 00:57 from IEEE Xplore. Restrictions apply.

species and high level injection of hot electrons into the anode.

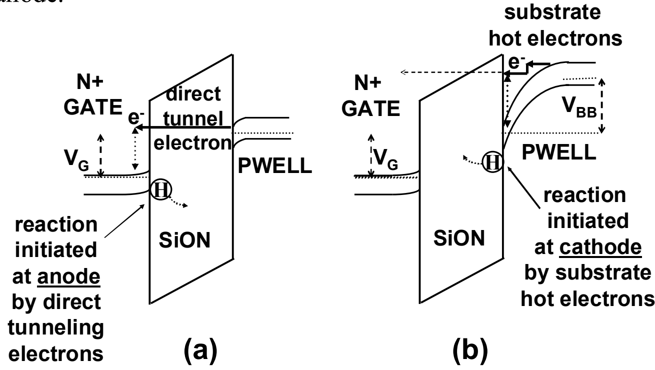

Figure 8. Band diagram for stress. Reaction initiated: (a) At anode, drawn with V_{BB} = 0V; (b) At cathode, $|V_{BB}|$ > 0V. Dashed horizontal arrow in (b) denotes transmission through the barrier. After Nicollian, Ref. [20].

The change in capacitance ΔC resulting from stress of 12Å SiON films with V_{BB} = -6V, V_G = +2.32V is plotted vs. V_G in Figure 9. Two trap peaks are seen. The area under the ΔC vs. V_G curve is charge. As the sum of the charge $Q_1 + Q_2 \sim Q_{\Delta VT}$, both states are acceptor like (negatively charged when occupied). Because holes create only donor states in SiON at low stress voltages [16,21], holes are not involved in the reaction that creates interface traps when a back bias is applied. Therefore, the reactants are electrons and Si-H bonds.

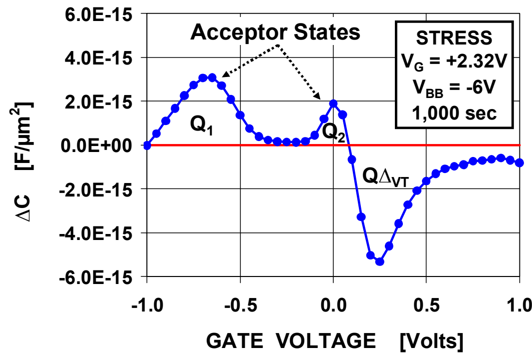

Figure 9. Change in capacitance after stress of 12Å SiON films with V_{BB} = -6V, V_G = +2.32V. The two trap peaks are acceptor states. After Nicollian, Ref. [20].

Using ΔI_{DLIN} as a measure for interface state generation, interface trap generation power laws for 12Å SiON films are plotted with V_{BB} as a parameter in Figure 10. The interface trap generation power law "m" increases to 0.38 for -6V V_{BB}, indicating that a charged species is involved. Figure 11 shows the effect of delay time on interface trap generation when a back bias is applied. The interrupted stress and uninterrupted stress curves are determined from LV-SILC [22] and ΔI_{DLIN} respectively. Since the power law exponent "m" is significantly larger for interrupted stress, recovery effects are present and the system is in quasi-equilibrium. Therefore, reaction-diffusion theory may be applied to the interface trap generation reactions. From Figures 9 and 10: (i) two acceptor traps are generated, (ii) the reactants are electrons and Si-H bonds, (iii) a charged species is released at the cathode. A model for the reaction steps that are consistent with these observations is shown in Figure 12 [20]. The 1/3 power law is driven by the desorption of H^- and H^0 by cathode hot electrons. Note that the steps leading to the final product H_2^- in Figure 12 is an "effective" reaction, as TCAD simulations show that a 1/3 power law can also arise from equal amounts of H^- and H^0. "m" slightly higher than 1/3 may be due to a higher desorption rate for H^- over H^0 when hot electrons impinge on the cathode interface. The existence of one form of charged H_2 in SiO_2 (H_2^+) has been proposed [23].

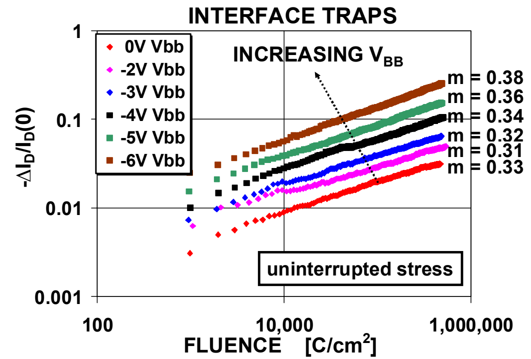

Figure 10. Change in I_{DLIN} after stress of 12Å SiON with V_{BB} = -6V, V_G = +2.32V. After Nicollian, Ref. [20].

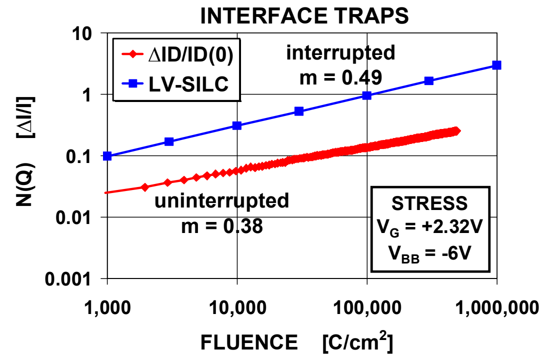

Figure 11. Interface trap generation power laws from LV-SILC (-1V sense) and ΔI_{DLIN} for interrupted vs. uninterrupted stress respectively. 12Å SiON films were stressed at V_G = +2.32V and V_{BB} = -6V. Larger "m" for interrupted stress is due to recovery. After Nicollian, Ref. [20].

It is also possible to directly observe the reactions that initiate trap generation and breakdown at the Si-SiON interface by stressing in accumulation. However, this mode is more complicated to analyze because large numbers of holes are present, which introduce additional reaction possibilities.

Having established that application of a back bias releases H^0 and H^- from the cathode into the dielectric, the effects of these species on SiON bulk trap creation can be evaluated. The build-up of bulk traps is sensed by SILC [24]. Figure 13 compares bulk trap generation with and without back bias applied during stress. The trap generation "m" increases from 0.26 (V_{BB} = 0V) to 0.51 (V_{BB} = -6V). The bulk trap generation pre-factor "b" is lower at -6V V_{BB}, indicating that the -6V V_{BB}

Authorized licensed use limited to: PORTLAND STATE UNIVERSITY. Downloaded on May 22, 2009 at 00:57 from IEEE Xplore. Restrictions apply.

cathodic species released suppresses nominal bulk trap generation through a reaction that depletes the anodic species. Otherwise, the trap density would be the same or higher at all fluence. Accordingly, nominal bulk trap generation is due to the release of a positively charged anode species [20].

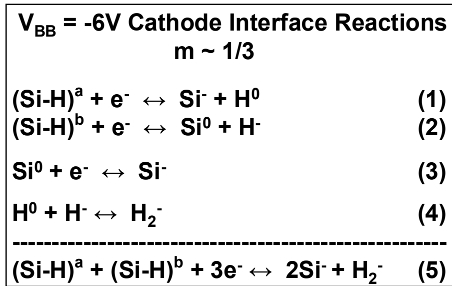

Figure 12. Model for cathode reactions for acceptor interface trap creation at -6V V_{BB} stress. (5) is the effective net reaction. $(Si\text{-}H)^a$ and $(Si\text{-}H)^b$ are precursors. After Nicollian, Ref. [20]

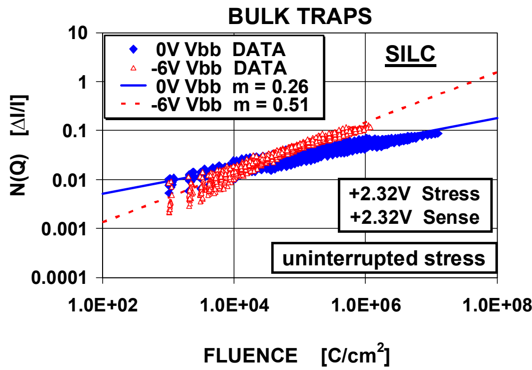

Figure 13. Bulk trap generation power laws for V_{BB} = 0V and V_{BB} = -6V stress. The devices are 12Å SiON films with V_G = +2.32V during stress and sense. The lines are statistical fits to the data. After Nicollian, Ref. [20].

In Figure 14, the V_{BB} dependence of the Weibull slope, which is a geometric quantity, rules out the transmission of substrate hot electrons into the anode (dashed horizontal line in Figure 8b) as the primary cause for the modifications in trap generation seen in Figure 13. The changes of Weibull slopes in Figure 14 are proportional to the changes in "m", consistent with predictions from the cell-based percolation model [25]. Comparison of the trend in Weibull slope with V_{BB} in Figure 14 with the trends in power law parameters with V_{BB} in Figure 15 shows that our trap generation power laws are tracking the traps that cause SBD.

A model for the nominal (V_{BB} = 0V) anode reactions are shown in Figure 16. Bulk traps are generated in the SiON dielectric by H^+ or H_2^+ following the desorption of Si-H bonds by anode hot holes. The hot holes originate through impact ionization of electrons tunneling in to the anode. A 2ND anode reaction that releases H^0 is also needed to account for nominal cathode interface trap creation because only neutral or positive species can be released from the anode into the dielectric and H^+ is not highly reactive at Si-SiO_2 interfaces [23]. Moreover, positive species create donor traps at the Si-SiON interface, but acceptor states are still the dominant cathode interface traps when V_{BB} = 0V as shown in Figure 17. The differences in V_G dependence and trap generation rate between SILC and LV-SILC indicate that bulk and interface trap generation are not triggered by the same reaction [20]. Although H^0 may be liberated from nominal bulk trap creation (m ~ 0.25 for V_{BB} = 0V; see Figures 7 and 13), this cannot be the sole source of H^0 since the generation rate is higher for interface traps [20]. A band diagram for trap creation is shown in Figure 18. Both H^+ and H^0 create interface traps at the anode when they are released. After entering the dielectric, H^+ subsequently creates SiON bulk traps and H^0 creates cathode interface traps [20].

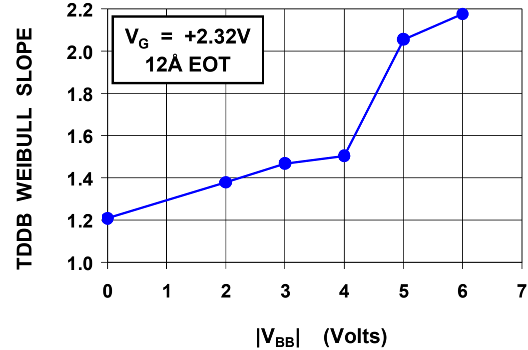

Figure 14. TDDB Weibull slope vs. $|V_{BB}|$ for 12Å SiON films stressed at V_G = +2.32V. After Nicollian, Ref. [20].

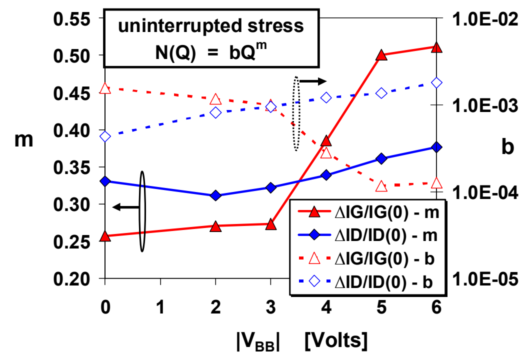

Figure 15. Trap generation power law parameters for 12Å SiON films stressed at V_G = +2.32V. $\Delta I_G/I_G(0)$ and $\Delta I_D/I_D(0)$ represent bulk and interface trap generation respectively. After Nicollian, Ref. [20].

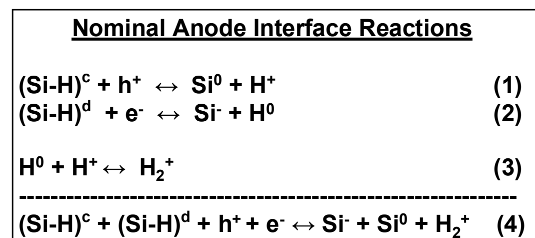

Figure 16. Model for nominal anode reactions. H^+ is desorbed by holes and H^0 is desorbed by electrons. (4) is the net effective reaction. $(Si\text{-}H)^c$ and $(Si\text{-}H)^d$ are precursors. After Nicollian, Ref. [20].

Authorized licensed use limited to: PORTLAND STATE UNIVERSITY. Downloaded on May 22, 2009 at 00:57 from IEEE Xplore. Restrictions apply.

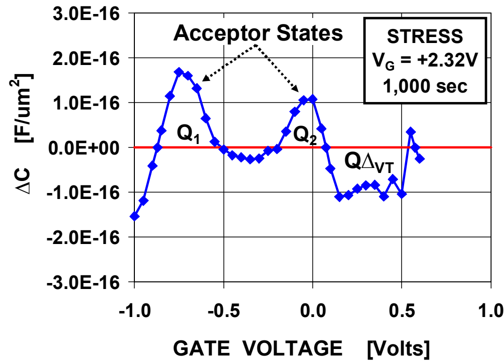

Figure 17. Change in capacitance after stress of 12Å SiON films at V_G = +2.32V, V_{BB} = 0V. Two acceptor trap peaks are also seen after 0V V_{BB} stress. After Nicollian, Ref. [20].

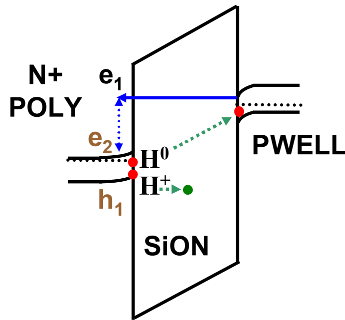

Figure 18. Model for trap generation in SiON. e_1 tunnels into the anode, impact ionizes, and creates e_2 and h_1. H^+ and H^0 are subsequently desorbed. H^+ generates bulk and poly-SiON interface traps. H^0 generates traps at both interfaces. After Nicollian, Ref. [20].

Comparison of the behavior of breakdown data with scanning tunneling microscopy results

Many of the recent breakthroughs regarding the role of hydrogen in trap generation and breakdown in MOS devices have been leveraged from scanning tunneling microscopy (STM) experiments. In this section, we review the features of STM that are central to the current understanding of oxide breakdown and show that the results of these studies leads to an explanation to the TDDB Power Law Model.

There are two silicon-hydrogen bond desorption mechanisms that we will consider: Electrical excitation (EE) and vibrational excitation (VE). Electrical excitation is a process where hydrogen is desorbed via field emission [14]. EE has a threshold energy of 6eV to 7eV and is weakly dependent on energy and current. [14]. Vibrational excitation is a process where hydrogen is desorbed via excitation of phonon modes [14,26-29]. VE is an important mechanism in the Si-SiO_2 system because the Si-H bond has a long vibrational lifetime; on the order of 10^{-8} seconds [14]. VE can occur at energies below the threshold energy for EE since E_{TH} for VE is about 2.5eV to 3.0eV. Since the phonon modes are about $\hbar\omega$ = 0.25eV apart, there $E_{TH}/0.25 \sim$ 10 to 12 levels between the ground state and the top of the potential well [14]. The mechanisms for vibrational excitation are shown in Figure 19 as follows: (a) one electron coherent excitation. This occurs when a single electron desorbs the Si-H bond from the ground state [26]. This process is strongly dependent on voltage and weakly dependent on current. (b) Incoherent vibrational excitation [27,28]. In this process, the Si-H bond is desorbed via 10-12 electrons (1 per energy level) and occurs when incoming electrons have energies < $2\hbar\omega$. The rate of this process is extremely small. Incoherent vibrational excitation is strongly dependent on voltage and current. The strong current dependence for multi-vibrational hydrogen release (MVHR) arises from the higher probability of desorption when large numbers of electrons are present. (c) Multi-electron excitation, where only a few electrons are needed for hydrogen release [29]. For M electrons, the energy per electron for desorption to occur is $\geq E_{TH}/M$. Accordingly, MVHR also occurs at energies below the threshold energy for VE, albeit at a lower probability than single electron desorption. However, MVHR involving only 2 or 3 electrons is significantly more probable than incoherent excitation and can play an important role below 2.5eV. The voltage and current dependences of EE and VE processes are tabulated in Figure 20.

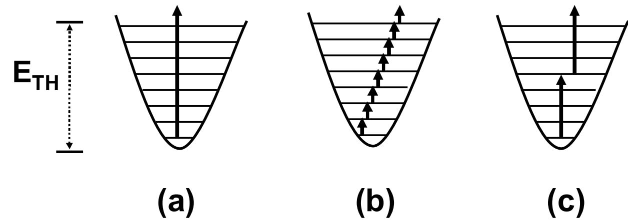

Figure 19. Vibrational excitation processes. (a) Single electron coherent excitation. (b) Incoherent excitation. (c) Two electron excitation.

HR Mechanism	Current Dependence	Voltage Dependence
EE	WEAK	WEAK
COHERENT VE	WEAK	STRONG
MULTI-ELECTRON VE	STRONG	STRONG
INCOHERENT VE	STRONG	STRONG

Figure 20. Summary of voltage and current dependence of electrical and vibrational excitation processes.

Yield vs. voltage for hydrogen desorption measured in STM experiments is shown in Figure 21. The plateau of the curve is the EE regime. In the region where the yield is rapidly decreasing with voltage, VE becomes an important mechanism. Since the TDDB Power Law Model has a strong voltage dependence, electrical excitation is ruled out as the mechanism that results in the TDDB Power Law Model.

The voltage dependence of the fraction of tunneling electrons that excite a silicon hydrogen phonon mode is shown in Figure 22. It can be seen that this inelastic tunneling fraction has a power law dependence of V^4 (per level) [14]. Accordingly, the inelastic tunneling fraction has a net voltage dependence of V^{4n}, which is V^{40-48} for 10 to 12 phonon

Authorized licensed use limited to: PORTLAND STATE UNIVERSITY. Downloaded on May 22, 2009 at 00:57 from IEEE Xplore. Restrictions apply.

levels. Therefore, vibrational excitation of hydrogen provides a plausible mechanism for the TDDB Power Law Model [28]. The general form of the voltage and current dependence for the generation efficiency of vibrational excitation processes involving M electrons is [29]

$$\xi(V,I) = I_0^{M-1} V^{4N} \quad (11)$$

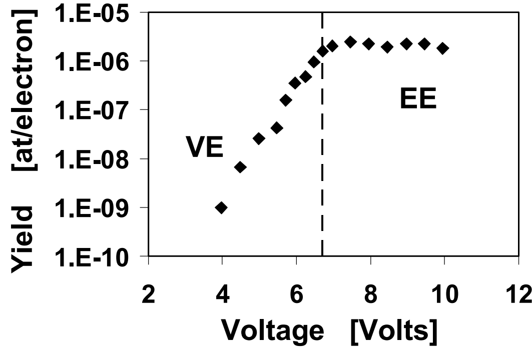

Figure 21. STM Yield vs. voltage for hydrogen desorption. After Shen, Ref. [14].

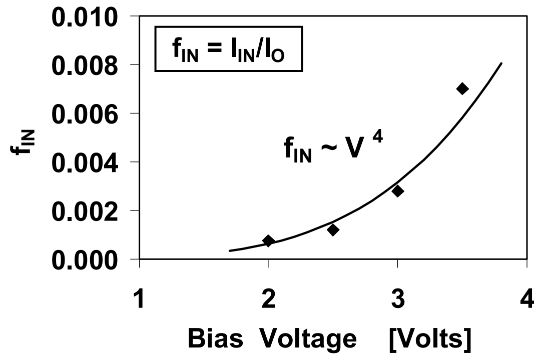

Figure 22. Inelastic tunneling fraction vs. bias voltage from STM experiments. Data plotted is from Shen, Ref. [14].

We will now compare trap generation and breakdown data to STM results. One of the difficulties in resolving single vs. multi-electron desorption is that the effects of current, which is a function of voltage, must be decoupled from the voltage. Because substrate hot electron injection (SHE) can be used to independently control oxide electric field, electron energy, and electron fluence [31], this technique can be applied to the studies vibrational excitation mechanisms. Using SHE, interface trap generation has been reported to be dependent on gate current at low voltages [32], indicating the presence of MVHR as a mechanism for interface trap generation at the cathode interface. These findings indicate that behavior reported in STM experiments also occurs under electrical stress in MOS devices.

The current and voltage dependence of trap generation and breakdown can also be separated by stressing oxides of different thickness at the same voltage [30]. From (11), the trap generation efficiency ξ should be independent of current for single electron VE so that ξ vs. E_{MAX} should be independent of thickness. For two electron VE, ξ/J vs. E_{MAX} should be independent of thickness [30]. For $E_{MAX} > 2.5$eV, the data corresponding to $\xi(E_{MAX})$ for different thickness fall on the same curve in Figure 23. Accordingly, these data are consistent with single electron vibrational excitation. For $E_{MAX} < 3.0$eV, the data corresponding to $\xi/J(E_{MAX})$ fall on the same curve in Figure 24. Therefore, below the 2.5eV to 3.0eV threshold energy for vibrational excitation, trap generation and breakdown are consistent with 2 electron VE.

Figure 24 yields a power law $\xi/J \sim E_{MAX}^{41}$ for $E_{MAX} < 2.5$eV and Figure 23 yields a power law $\xi \sim E_{MAX}^{35}$ for $E_{MAX} > 2.5$eV. The power law exponent decreases as E_{MAX} increases and goes to zero as HR transitions towards the EE regime. This suggests that EE and VE may cooperate in the intermediary region between 2.5eV and 7.0eV [30]. Since a vibrational excitation increases the S-H bond distance, the threshold energy for desorption should decrease proportionally [33]. In this scenario, one electron excites the bond to a vibrational state, followed by an electrical excitation event that desorbs the hydrogen. While the symmetric harmonic oscillator potentials in Figure 19 provide a useful visualization of vibrational excitation processes, they do not capture cooperative processes between EE and VE via an increase in bond length. A Morse potential, which is asymmetric, has been used to model this behavior [30].

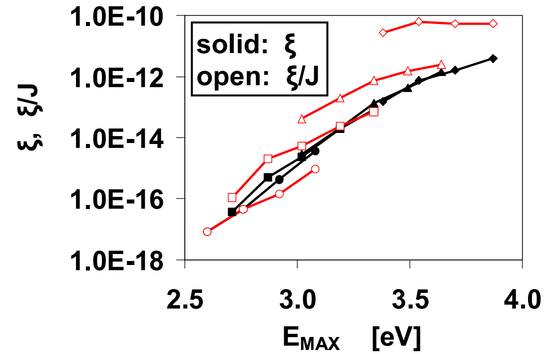

Figure 23. Trap generation efficiency (ξ) and ξ/J vs. E_{MAX} for $E_{MAX} > 2.5$eV. The oxide thicknesses are 19Å (circles), 23Å (squares), 25Å (triangles), and 29Å (diamonds). The data are consistent with single electron VE. After Suñé, Ref. [30].

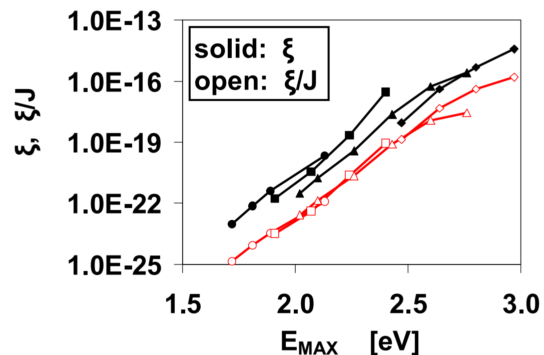

Figure 24. Trap generation efficiency (ξ) and ξ/J vs. E_{MAX} for $E_{MAX} < 3.0$eV. The oxide thicknesses are 13.8Å (circles), 15Å (squares), 16.7Å (triangles), and 18.7Å (diamonds). The data are consistent with 2 electron VE. After Suñé, Ref. [30].

Authorized licensed use limited to: PORTLAND STATE UNIVERSITY. Downloaded on May 22, 2009 at 00:57 from IEEE Xplore. Restrictions apply.

Voltage and temperature dependence of trap generation

In this section, we will present additional experimental evidence that two hydrogen species are released during TDDB stress through two separate anode reactions. We will also show additional results that support a transition from single to multiple vibrational excitation as the mechanism that causes breakdown. We will then discuss the influence of desorption mechanisms on the traps that cause breakdown.

We will begin this section with a discussion on the voltage dependence of trap generation and breakdown. The voltage acceleration factor for Q_{BD} is written as:

$$AF(Q_{BD}) = -\partial \ln(Q_{BD})/\partial V_G \qquad (12)$$

Solving equation (10) for $Q = Q_{BD}$:

$$Q_{BD} = (N_{BD}/b)^{1/m} \qquad (13)$$

Where N_{BD} is the trap density at breakdown. Inserting (13) into (12) and assuming that N_{BD} is independent of V_G, we get:

$$AF(Q_{BD}) = (1/m)\, \partial \ln b/\partial V_G \qquad (14)$$

The trap density N(Q) in (10) is obtained from SILC and LV-SILC measurements. Note that it is not necessary to stress to breakdown to extract the voltage dependence of trap generation because the V_G dependence is carried solely in the trap generation pre-factor "b". The voltage acceleration factors for Q_{BD}, SILC, and LV-SILC are plotted in Figure 25. For all stress conditions, the acceleration factors for SILC and LV-SILC are sharply different. This confirms the two reaction model proposed in Figures 16 and 18. A transition from bulk trap limited to interface state limited breakdown occurs at about 2.7V, as AF(SILC) tracks AF(Q_{BD}) above 2.7V and AF(LV-SILC) tracks AF(Q_{BD}) below 2.7V [34]. This transition coincides with E_{TH} for multi-vibrational hydrogen release. As bulk traps are generated by H^+, the reduced role of H^+ relative to H^0 may be due to the higher bias and current required for hole induced multi-carrier vibrational excitation [35]. Accordingly, below 2.7V, breakdown is controlled by electron induced desorption of H^0 [34].

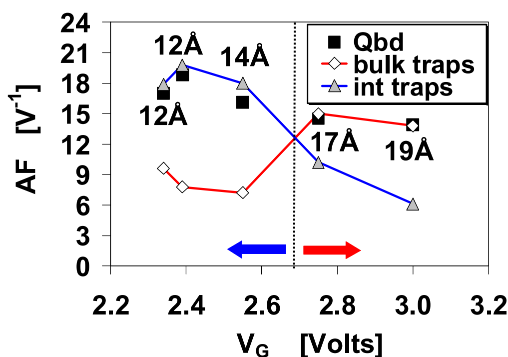

Figure 25. AF for Q_{BD}, SILC, and LV-SILC. A transition from bulk to interface trap controlled breakdown occurs below 2.7V. After Nicollian, Ref. [34].

We now link the temperature dependence of breakdown to trap generation. We will assume that Q_{BD}, "m", and "b" follow Arrhenius relationships with activation energy ΔH.

$$\Delta H(N_{BD}) = -k_B * \partial \ln N_{BD}/\partial(1/T) \qquad (15)$$

$$\Delta H(b) = -k_B * \partial \ln b/\partial(1/T) \qquad (16)$$

$$\Delta H(Q_{BD}) = -k_B * \partial \ln Q_{BD}/\partial(1/T) \qquad (17)$$

Inserting (13), (15), and (16) into (17), the activation energy for breakdown becomes [34]:

$$\Delta H(Q_{BD}) = (1/m)*[\Delta H(N_{BD}) - \Delta H(b)] \qquad (18)$$

Unlike the V_G dependence, oxides must be stressed to breakdown to tie together the temperature dependence of trap generation and breakdown. The temperature dependence of Q_{BD} for 13Å SiON films with 10^{-7} cm^2 gate areas stressed at +2.2V is shown in Figure 26. The data fit an Arrhenius relationship between 75°C to 150°C. N_{BD} and "b" also follow an Arrhenius relationship in this temperature range [34]. The results are tabulated in Figure 27 and confirm that interface traps are the defects that control breakdown at low V_G.

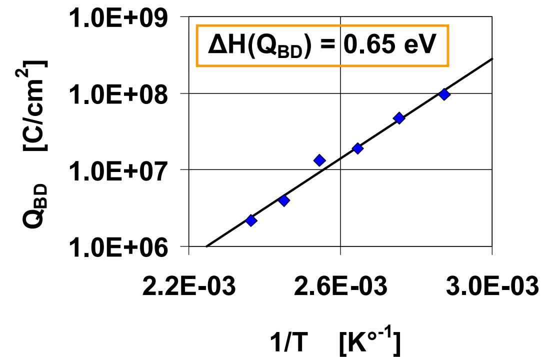

Figure 26. Arrhenius plot for Q_{BD}. 13Å SiON films with 10^{-7} cm^2 gate areas are stressed at +2.2V from 75°C to 150°C. After Nicollian, Ref. [34].

ΔH directly from Q_{BD}	ΔH from SILC (bulk traps)	ΔH from LV-SILC (interface traps)
0.65 eV	0.12 eV	0.66 eV

Figure 27. ΔH from breakdown and trap generation measurements using equations (15) – (18). The temperature data verify that interface traps control breakdown. After Nicollian, Ref. [34].

Our experimental values of the trap generation power law exponent 'm" are about 0.3 [20,34]. This is smaller than the 0.5 to 1.0 values that are often reported in the literature [25,36]. However, our experimentally obtained m ~ 0.3 provides a match between the voltage and temperature dependence of trap generation with breakdown. It has been

Authorized licensed use limited to: PORTLAND STATE UNIVERSITY. Downloaded on May 22, 2009 at 00:57 from IEEE Xplore. Restrictions apply.

reported that bulk trap N_{BD} is time dependent when $t_{63\%} > 10^6$ seconds [37]. However, our mean stress times are significantly less than this. The process conditions in [37] were not specified.

Anode hole injection at low voltages

We now evaluate whether AHI is a viable mechanism for breakdown at low V_G in inverted NMOS devices. Since the n+ doped poly silicon anode is depleted under low voltage stress conditions, we examine whether there are sufficient numbers of free holes available for minority ionization. The number of holes is plotted vs. temperature in Figure 28. The effects of band gap narrowing due to high doping [38] are included and it is assumed that the bands are bent to the intrinsic condition ($\varphi = \varphi_B$) and the poly depletion region width is X_{DMAX}. Since the poly band bending at stress conditions is less than $E_G/2$ even for degenerate doping and since X_D is actually less than X_{DMAX}, the intrinsic concentration of holes shown in Figure 28 is an overestimate of the actual number. It can be seen that even for the highest doping concentration, the temperature must exceed 80°C for there to be 1 free hole in a 10μm^2 gate area that is typical of the devices that were stressed. Therefore, anode hole injection through minority ionization in inverted NMOS is improbable at low V_G.

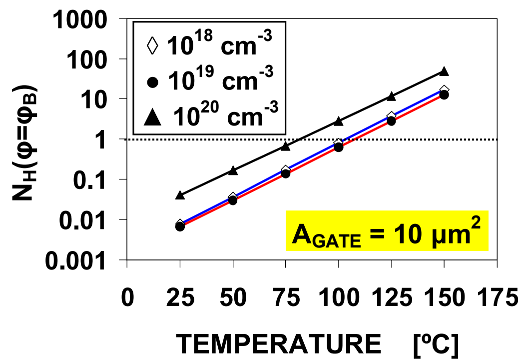

Figure 28. Calculated number of holes vs. temperature for inverted NMOS devices with 10 μm^2 gate area, with the poly doping density as a parameter.

We will now investigate whether AHI through majority ionization is the mechanism for breakdown at low gate voltage. A band diagram for AHI for NMOS stressed in inversion is shown in Figure 29. It can be seen that there is insufficient energy to inject holes over the barrier. However, this by itself does not rule out AHI because inelastic scattering could result in a high energy tail. As shown in Figure 17, the interface traps created are primarily acceptor states. Because holes create donor states, AHI is ruled out as the mechanism for interface trap generation. Since we have shown that interface traps control breakdown in Figures 25 and 27, AHI is ruled out as the mechanism for low voltage breakdown.

Implications for thickness scaling

We will now explore the roles of bulk and interface traps on the formation on SBD percolation paths in SiON dielectrics. Weibull slopes for EOT < 22Å are shown in Figure 30 [34]. While the thickness dependence is weak, it is still apparent down to 10Å EOT. The continuing scalability of β with thickness implies that at least two traps are still needed to form a SBD path down to 10Å. The t_{OX} dependence of β is not unique because both the physical thickness and nitrogen profiles are modified to scale EOT. We will apply the cell-based approach [25] to analyze this problem. A simple relation between β and t_{OX} arises from this model [25]:

$$\beta = m t_{OX}/a_0 \quad (19)$$

In equation (19), a_0 is the defect size. A percolation path formed by 2 interface traps at the maximum oxide thickness (arbitrarily, $5a_0$ that this can occur) is shown in Figure 31a. Figure 31b shows the possible percolation paths involving only interface traps with $t_{OX} = 4a_0$. From (19) and Figures 31a and 31b, a model involving only interface traps does not capture the observed thickness dependence of β shown in Figure 30 since the number of traps in the percolation path is always two. Therefore, while the generation of interface traps is the rate limiting step, at least one bulk trap must be involved to capture the correct thickness scaling trend [34]. A possible scenario involving both bulk and interface traps in the percolation path and exhibiting the correct t_{OX} scalability of β is shown in Figure 32.

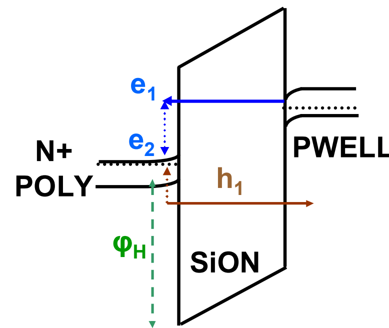

Figure 29. Band diagram at low V_G for minority ionization in depleted NMOS poly with the device stressed in inversion.

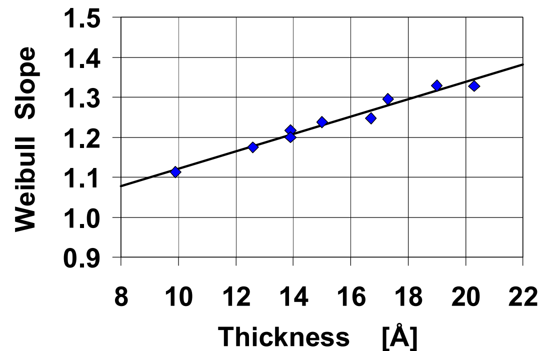

Figure 30. TDDB Weibull slope vs. thickness for SiON dielectrics. After Nicollian, Ref. [34].

In the cell based approach, the trap size a_0 is determined by the slope of β vs. t_{OX}. Since $\beta \neq 0$ at $t_{OX} = 0$, the existence of an interfacial layer that offsets the oxide thickness has been proposed [25]. However, since a mixture of bulk and interface

Authorized licensed use limited to: PORTLAND STATE UNIVERSITY. Downloaded on May 22, 2009 at 00:57 from IEEE Xplore. Restrictions apply.

traps are required for breakdown, a single defect size will not be extracted from the slope. Instead, we find the instantaneous value of a_0 for each β. When plotted against thickness, a_0 asymptotically approaches its bulk value as t_{OX} increases, as shown in Figure 33 [34]. Using m = 0.26 [20], the bulk trap diameter is about 4Å, resulting in the Weibull slope remaining thickness dependent and > 1 down to 10Å EOT.

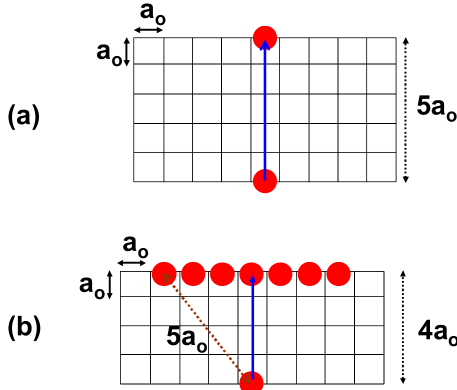

Figure 31. Schematic for 2-trap percolation involving only interface traps for (a) $t_{OX} = 5a_0$. (b) $t_{OX} = 4a_0$ with $d = 5a_0$. This model does not explain the thickness scaling of β in Figure 30. After Nicollian, Ref. [34].

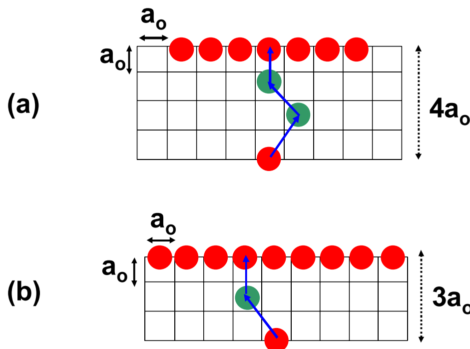

Figure 32. Schematic for 2-trap percolation involving both interface and bulk traps for (a) $t_{OX} = 4a_0$. (b) $t_{OX} = 3a_0$. This model is consistent with the thickness scaling of β in Figure 30. After Nicollian, Ref. [34].

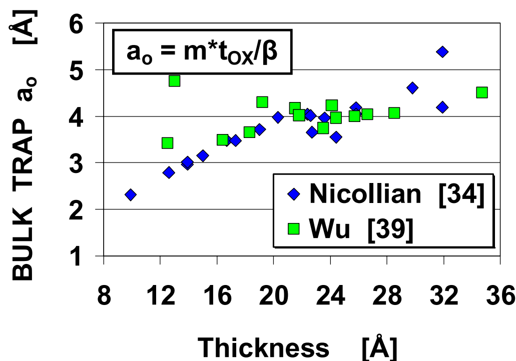

Figure 33. Bulk trap diameter vs. t_{OX} using the cell based approach. For m = 0.26 [20], the asymptotic value of a_0 at large thickness is about 4Å. After Nicollian, Ref. [34].

CONCLUSIONS

In small area devices at low stress voltages, there are insufficient numbers of holes in depleted NMOS poly for anode hole injection through minority ionization to be a significant degradation mechanism. Anode hole injection through majority ionization is further eliminated as the mechanism for NMOS SBD when the rate limiting step for breakdown is the generation of acceptor-like interface traps.

Reaction-diffusion theory applies to $+V_G$ stress of ultra-thin NMOS SiON films. Measurable recovery effects are present, showing that quasi-equilibrium exists for NMOS TDDB. This allows the determination of the reactions that result in anode hydrogen release.

Both holes and electrons are involved in the desorption of hydrogen at the anode. Trap generation is triggered by the release of two hydrogen species (H^+ and H^0) in two separate anode reactions. Both species create interface traps at the poly interface when they are released. After migrating into the dielectric, H^+ subsequently creates bulk traps and H^0 creates pwell interface traps. The hydrogen species that controls breakdown is voltage dependent.

The trap generation efficiency during electrical stress tracks the results from STM experiments of H^0 desorption. A transition from a one electron to two electron VE process below about 2.5V is deduced from Q_{BD} data. A transition from bulk to interface trap limited breakdown occurs at 2.7V, which also coincides with the threshold voltage for vibrational excitation of silicon-hydrogen bonds.

A power law dependence of the time to breakdown on gate voltage only occurs when the hydrogen desorption mechanism is VE. The TDDB power law exponent N > 40 arises from the voltage dependence of the fraction of tunneling electrons that excite a silicon-hydrogen phonon mode.

While the generation of interface states becomes the rate limiting step below the threshold energy for VE, both bulk and interface traps are still required for breakdown to occur. A minimum of two traps is needed to cause breakdown down to 10Å EOT. At least one trap must be an interface state and at least one must be a bulk state.

While there are some discrepancies in the literature regarding bulk trap size, our results lead to a bulk trap diameter of about 4Å. This is the smallest estimate bulk trap size reported to date, and results in the Weibull slope remaining thickness dependent and > 1 down to 10Å EOT (for $t_{PHYSICAL} \geq 12$Å). Our extracted bulk trap size of 4Å is in part consequent of our experimentally obtained trap generation power law exponent "m" being about 0.3. This is smaller than the values that are typically quoted in the literature, and provides a consistent explanation for the voltage, temperature, and thickness dependence of breakdown.

In summary, the experiments reviewed in this paper show that the TDDB power law model is on reasonably solid experimental ground.

ACKNOWLEDGEMENTS

The authors would like to thank Srikanth Krishnan and James Ondrusek for their support of this work.

Authorized licensed use limited to: PORTLAND STATE UNIVERSITY. Downloaded on May 22, 2009 at 00:57 from IEEE Xplore. Restrictions apply.

REFERENCES

[1] Semiconductor Industry Association, *The International Technology Roadmap for Semiconductors*, 2001 edition, International Sematech: Austin, TX 2001. Semiconductor Industry Association, *The International Technology Roadmap for Semiconductors*, 2004 update, International Sematech: Austin, TX 2004

[2] E.Y. Wu, et. al., "Voltage Dependent Voltage Acceleration of Oxide Breakdown for Ultra-thin Oxides", *IEDM Technical Digest*, 541 (2000)

[3] D.J. DiMaria and J.W. Stasiak, "Trap Creation in Silicon Dioxide Produced by Hot Electrons", *Journal of Applied Physics*, **65**, 2342 (1989)

[4] I.C. Chen, S. Holland, K.K Young, and C. Hu, "Substrate Hole Current and Oxide Breakdown", *Applied Physics Letters*, **49**, 669 (1986)

[5] K.F. Schuegraf and C. Hu, "Hole Injection in SiO_2 Breakdown Model for Very Low Voltage Lifetime Extrapolation", *IEEE Transactions* on Electron Devices, **41**, 761 (1994)

[6] D.J. DiMaria, "Explanation for the Polarity Dependence of Breakdown in Ultra thin Silicon Dioxide Films", *Applied Physics Letters*, **68**, 3004 (1996)

[7] P.E. Nicollian, W.R. Hunter, and J. Hu, "Experimental Evidence for Voltage Driven Breakdown Models in Ultra thin Gate Oxides", *Proceedings of the IRPS,* 7 (2000)

[8] E.M. Vogel, J.S. Suehle, M.D. Edelstein, B. Wang, Y. Chen, and J.B. Bernstein, "Reliability of Ultra thin Silicon Dioxide under Combined Substrate Hot Electron and Constant Voltage Tunneling Stress", *IEEE Transactions on Electron Devices*, **47**, 1183 (2000)

[9] D. Wolters and J.F. Verwey, *Instabilities in Silicon Device*s, Volume 1, edited by G. Barbottin and A. Vapaille, North Holland: Elsevier Science Publishers B.V., 1986, pp. 315-362

[10] S. Ogawa, N. Shiono, and M. Shimaya, "Neutral Electron Trap Generation in SiO_2 by Hot Holes", *Applied Physics Letters*, **56**, 1329 (1990)

[11] J.F. Zhang, C.Z. Zhao, A.H. Chen, G. Groeseneken, and R. Degraeve, "Hole Traps in Silicon Dioxides – Part I: Properties", *IEEE Transactions* on Electron Devices, **51**, 1267 (2004)

[12] S.K. Lai, "Interface Trap Generation in Silicon Dioxide when Electrons are Captured by Trapped Holes", *Journal of Applied Physics*, **54**, 2540 (1983)

[13] J.D. Bude, B.E. Weir, and P.J. Silverman, "Explanation of Stress Induced Damage in Thin Oxides", *IEDM Technical Digest*, 179 (1998)

[14] T.C. Shen, et. al., "Atomic Scale Desorption through Electronic and Vibrational Excitation Mechanisms", *Science*, **268**, 1590 (1995)

[15] K.O. Jeppson and C.M. Svensson, "Negative Bias Stress of MOS Devices at High Electric Fields and Degradation of MNOS Devices", *Journal of Applied Physics*, **48**, 2004 (1977)

[16] A.T. Krishnan, et. al., "Material Dependence of Hydrogen Diffusion: Implications for NBTI Degradation", *IEDM Technical Digest*, 705 (2005)

[17] S. Chakravarthi, A.T. Krishnan, V. Reddy, C.F. Machala, and S. Krishnan, "A Comprehensive Framework for Predictive Modeling of Negative Bias Temperature Instability", *Proceedings of the IRPS,* 273 (2004)

[18] M.A. Alam, "NBTI: Modeling", *IRPS Tutorials*, 211 (2005)

[19] S. Ogawa and N. Shiono, "Generalized Diffusion-Reaction Model for the Low-Field Charge Buildup Instability at the Si-SiO_2 Interface", *Physical Review B*, **51**, 4218 (1995)

[20] P.E. Nicollian, A.T. Krishnan, C. Bowen, S. Chakravarthi, C.A. Chancellor, and R.B. Khamankar, "The Roles of Hydrogen and Holes in Trap Generation and Breakdown in Ultra thin SiON Dielectrics", *IEDM Technical Digest*, 403 (2005)

[21] V.K. Reddy, et. al., "Impact of Negative Bias Temperature Instability on Digital Circuit Reliability", *Proceedings of the IRPS,* 248 (2002)

[22] P.E. Nicollian, M. Rodder, D.T. Grider, P. Chen, R.M. Wallace, and S.V. Hattangady, "Low Voltage Stress Induced Leakage Current in Ultra thin Gate Oxides", *Proceedings of the IRPS,* 400 (1999)

[23] S. Pantelides, S.N. Rashkeev, R. Buczko, D.M. Fleetwood, and R.D. Schrimpf, "Reactions of Hydrogen with Si-SiO_2 Interfaces", *IEEE Transactions on Nuclear Science*, **47**, 2262 (2000)

[24] D.J. DiMaria and E. Cartier, "Mechanisms for Stress Induced Leakage Currents in Thin Silicon Dioxide Films", *Journal of Applied Physics*, **78**, 3883 (1995)

[25] J. Suñé, "New Physics Based Analytic Approach to the Thin Oxide Breakdown Statistics", *IEEE Electron Device Letters*, **22**, 296 (2001)

[26] G.P. Salam, M. Persson, and R.E. Palmer, "Possibility of Coherent Multiple Excitation in Atom Transfer with a Scanning Tunneling Microscope", *Physical Review B*, **49**, 10655 (1994)

[27] R.E. Walkup, D.M. Newns, and Ph. Avouris, "Role of Multiple Inelastic Transitions in Atom Transfer with the Scanning Tunneling Microscope" *Physical Review B*, **48**, 1858 (1993)

[28] W. McMahon, A. Haggag, and K. Hess, "Reliability Scaling Issues for Nanoscale Devices", *IEEE Transactions on Nanotechnology*, **2**, 33 (2003)

[29] B.C. Stipe, M.A. Rezaei, and W. Ho, "Single Molecule Dissociation by Tunneling Electrons", *Physical Review Letters*, **78**, 4410 (1997)

[30] J. Suñé and E.Y. Wu, "Mechanisms of Hydrogen Release in the Breakdown of SiO_2 Based Gate Oxides", *IEDM Technical Digest*, 399 (2005)

[31] D.J. DiMaria, "Defect Generation under Substrate Hot Electron Injection into Ultra thin Silicon Dioxide Layers", *Journal of Applied Physics*, **86**, 2100 (1999)

[32] G. Ribes, S. Bruyere, M. Denais, D. Roy, and G. Ghibaudo, "MVHR (Multi-Vibrational Hydrogen Release): Consistency with Bias Temperature Instability and Dielectric Breakdown", *Proceedings of the IRPS,* 377 (2005)

Authorized licensed use limited to: PORTLAND STATE UNIVERSITY. Downloaded on May 22, 2009 at 00:57 from IEEE Xplore. Restrictions apply.

[33] Ph. Avouris, et. al., "STM Induced H Atom Desorption from Si (100): Isotope Effects and Site Selectivity", *Chemical Physics Letters*, **25**7, 148 (1996)
[34] P.E. Nicollian, A.T. Krishnan, C.A. Chancellor, and R.B. Khamankar, "The Traps that cause Breakdown in Deeply Scaled SiON Dielectrics", *IEDM Technical Digest*, 743 (2006)
[35] K. Stokbro, et. al., "STM Induced Hydrogen Desorption via a Hole Resonance", *Physical Review Letters*, **80**, 2618 (1998)
[36] R. Degraeve, G. Groeseneken, R. Bellens, M. Depas, and H.E. Maes, "A Consistent Model for the Thickness Dependence of Intrinsic Breakdown in Ultrathin Oxides", *IEDM Technical Digest*, 863 (1995)
[37] J.H. Stathis, "Physical and Predictive Models of Ultra Thin Oxide Reliability", *Proceedings of the IRPS,* 132 (2001)
[38] S.M. Sze, *Physics of Semiconductor Devices*, 2ND edition, New York: Wiley, 1981, pp. 143-144
[39] E.Y. Wu, E. Nowak, and W. Lai, "Off-State Mode TDDB Reliability for Ultra-thin Gate Oxides: New Methodology and the Impact of Oxide Thickness Scaling", *Proceedings of the IRPS,* 84 (2004)

Authorized licensed use limited to: PORTLAND STATE UNIVERSITY. Downloaded on May 22, 2009 at 00:57 from IEEE Xplore. Restrictions apply.